Mon. Not. R. Astron. Soc. **000**, **??**–**??** (0000) Printed 15 March 2010 (MN LATEX style file v2.2)

Decomposition of Spectra from Redshift Distortion Maps

Yong-Seon Song[1] and Issha Kayo[2]

[1] *Institute of Cosmology & Gravitation, University of Portsmouth, Portsmouth, PO1 3FX, UK*
[2] *Institute for the Physics and Mathematics of the Universe, University of Tokyo, 5-1-5 Kashiwanoha, Chiba 277-8582, Japan*

15 March 2010

ABSTRACT

We develop an optimized technique to extract density–density and velocity–velocity spectra out of observed spectra in redshift space. The measured spectra of the distribution of halos from redshift distorted mock map are binned into 2–dimensional coordinates in Fourier space so as to be decomposed into both spectra using angular projection dependence. With the threshold limit introduced to minimize nonlinear suppression, the decomposed velocity–velocity spectra are reasonably well measured up to scale $k = 0.07\,h\,\mathrm{Mpc}^{-1}$, and the measured variances using our method are consistent with errors predicted from a Fisher matrix analysis. The detectability is extendable to $k \sim 0.1\,h\,\mathrm{Mpc}^{-1}$ with more conservative bounds at the cost of weakened constraint.

Key words: cosmology: large-scale structure

1 INTRODUCTION

The evolution of large scale structure, as revealed in the clustering of galaxies observed in wide–deep redshift surveys has been one of key cosmological probes. Structure formation is driven by a competition between gravitational attraction and the expansion of space-time, which enables us to test our model of gravity at cosmological scales and the expansion of history of the Universe (Wang 2008; Linder 2008; Guzzo et al. 2008; Song & Percival 2009; Simpson & Peacock 2009; Guzik et al. 2010; McDonald & Seljak 2009; Stril et al. 2009; Bean & Tangmatitham 2010).

Maps of galaxies where distances have been measured from redshifts show anisotropic deviations from the true galaxy distribution (York 2000; Peacock 2001; Colless 2003; Hawkins 2003; Percival 2004; Zehavi 2005; Le Fèvre 2005; Tegmark 2006; Okumura 2008; Gaztanaga & Cabre 2008; Garilli 2008; Guzzo et al. 2008), because galaxy recession velocities include components from both the Hubble flow and peculiar velocities. In linear theory, a distant observer should expect a multiplicative enhancement of the overdensity field of tracers due to the peculiar motion along the line of sight (Davis & Peebles 1982; Kaiser 1987; Lilje & Efstathiou 1989; McGill 1990; Lahav et al. 1991; Hamilton 1992; Fisher et al. 1994; Fisher 1995). In principle, the observed spectra in redshift space can be decomposed into both density–density and velocity–velocity spectra using angular projection dependence (Song & Percival 2009; Percival & White 2008; White et al. 2009; Song et al. 2010). With a local linear bias, the real-space galaxy density field is affected, while the peculiar velocity term is not. In this paper, we attempt to extract velocity–velocity spectra as an unbiased tool to trace the history of structure formation.

A theoretical formalism (White et al. 2009) was derived for forecasting errors when extracting velocity–velocity spectra out of the observed redshift space distortion maps. However, it is not yet fully understood what the optimal technique is to practically decompose the spectra as theory predicts. We propose a statistical technique to extract it up to the limit of theoretical estimation. Our method utilizes the distinct angular dependence of density–density and velocity–veclocity spectra to decompose them from two–dimensional redshift power spectra, and is consistent with the theoretical estimate from Fisher matrix analysis.

We present the detailed formalism in the next section. The Fisher matrix analysis to decompose spectra is briefly reviewed, then we present the method to decompose spectra in an optimal way with mock data. We discuss statistical method to minimize the effect by nonlinear suppression.

2 PECULIAR VELOCITY POWER SPECTRA EXTRACTION

2.1 Theoretical Expectation of Decomposition Accuracy

The observed power spectrum in redshift space is decomposed into spectra of density fluctuations and peculiar velocity fields in real space. The observed power spectra in redshift space, $\tilde{P}$, is given by,

$$\begin{aligned}\tilde{P}(k,\mu,z) &= \Big\{P_{gg}(k,z) + 2\mu^2 r(k)\Big[P_{gg}(k,z)P_{\Theta\Theta}(k,z)\Big]^{1/2} \\ &+ \mu^4 P_{\Theta\Theta}(k,z)\Big\}G(k,\mu,\sigma_v), \qquad (1)\end{aligned}$$

where P_{gg} is the galaxy–galaxy density spectrum, $P_{\Theta\Theta}$ is the velocity–velocity spectrum (Θ is the divergence of velocity map in unit of aH), and μ denotes the cosine of the angle between orientation of the wave vector and the line of sight. Because this decomposition is valid only at large scale and when the rotation of the velocity field is negligible, we focus on modes of $k < 0.1\,h\,\mathrm{Mpc}^{-1}$ (Pueblas & Scoccimarro 2009). The cross-correlation coefficient

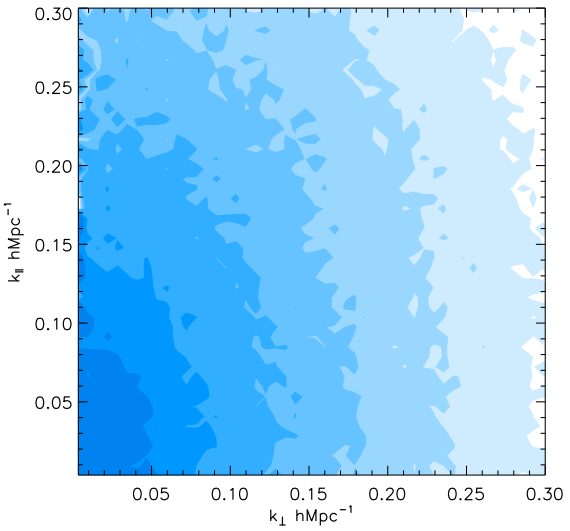

Figure 1. Power spectra from mock map in 2D cartesian coordinate $(k_\perp, k_\parallel)$.

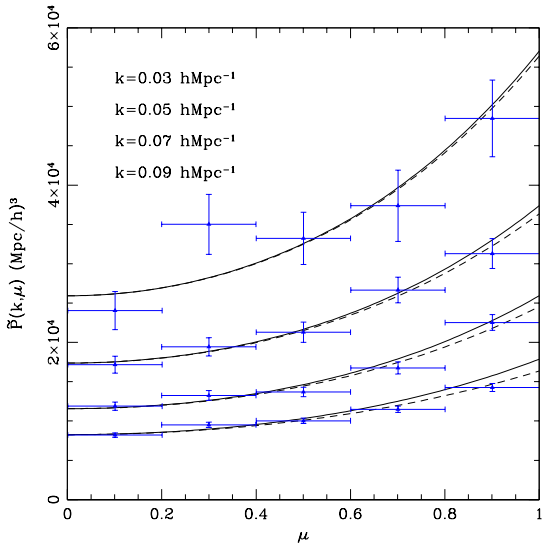

Figure 2. The observed power spectra at scales, $\bar{k}$=0.03, 0.05, 0.07 and 0.09 $h\,\mathrm{Mpc}^{-1}$ (from top to bottom) are plotted with error bars at various μ. Solid curves are $\tilde{P}_{\rm th}(k,\mu)$ (Kaiser effect alone) and dash curves are $\tilde{P}_{\rm fit}(k,\mu)$ (including dispersion effect) from best fitting bias $b(k)$.

$r(k)$ is defined as $r(k) \equiv P_{g\Theta}/\sqrt{P_{gg}P_{\Theta\Theta}}$. The density and velocity divergence are highly correlated for $k < 0.1\,h\,\mathrm{Mpc}^{-1}$ so we assume that both are perfectly correlated, $r(k) \sim 1$ (White et al. 2009). Then the density-velocity cross-spectrum becomes the geometric mean of the two auto-spectra and we have only two free functions, P_{gg} and $P_{\Theta\Theta}$. As Scoccimarro (2004) clearly pointed out, the redshift space power spectrum is suppressed along line-of-sight due to the velocity dispersion of large-scale flow, and we follow his model by introducing a function $G = \exp(-k^2\mu^2\sigma_v^2)$ where σ_v will be calculated from linear theory. Considering the possibility that nonlinear dynamics, like Finger-of-Gods effect, might contaminate the power spectrum, we use this term to find a cut-off scale of μ to exclude data which could be affected strongly by nonlinear dynamics. Indeed, Taruya et al. (2009) pointed out that σ_v calculated by linear theory does not match with result from N-body simulations if one tries to model the power spectrum at $\gtrsim 0.1\,h\,\mathrm{Mpc}^{-1}$. This cut-off edge $\mu_{\rm cut}$ is defined by $\mu_{\rm cut} \equiv \sigma_{\rm th}/k\sigma_v$, where the value of $\sigma_{\rm th}$ will be discussed later.

We estimate the accuracy of decomposition of P_{gg} and $P_{\Theta\Theta}$ from $\tilde{P}$ using Fisher matrix analysis determining the sensitivity of a particular measurement. Fisher matrix for this decomposition, $F^{\rm dec}_{\alpha\beta}$, is written as,

$$F^{\rm dec}_{\alpha\beta} = \int_{-\mu_{\rm cut}}^{\mu_{\rm cut}} d\mu \int \frac{\partial\tilde{P}(k,\mu)}{\partial p_\alpha}\frac{\partial\tilde{P}(k,\mu)}{\partial p_\beta}\frac{V_{\rm eff}(\tilde{P})}{\tilde{P}(k,\mu)^2}\frac{k^2dk}{2(2\pi)^2}\,, \quad (2)$$

where $p_\alpha = (P_{gg}, P_{\Theta\Theta})$. The effective volume $V_{\rm eff}(\tilde{P})$ is given by,

$$V_{\rm eff}(\tilde{P}) = \left[\frac{n\tilde{P}}{n\tilde{P}+1}\right]^2 V_{\rm survey}\,, \quad (3)$$

where n denotes galaxy number density.

Derivative terms in Eq. (2) are given by,

$$\begin{aligned}\frac{\partial\ln\tilde{P}(k_i,\mu,z_j)}{\partial P_{gg}(k_i,z_j)} &= \frac{1}{\tilde{P}(k_i,\mu,z_j)}\left[1+\mu^2\sqrt{\frac{P_{\Theta\Theta}(k_i,z_j)}{P_{gg}(k_i,z_j)}}\right]\\ \frac{\partial\ln\tilde{P}(k_i,z_j)}{\partial P_{\Theta\Theta}(k_i,z_j)} &= \frac{\mu^2}{\tilde{P}(k_i,\mu,z_j)}\left[\sqrt{\frac{P_{gg}(k_i,z_j)}{P_{\Theta\Theta}(k_i,z_j)}}+\mu^2\right]. \quad (4)\end{aligned}$$

The diagonal elements of the inverse Fisher matrix indicate the estimated errors of decomposion accuracy. The variances of $P_{gg}(k_i,z_j)$ and $P_{\Theta\Theta}(k_i,z_j)$ is given by,

$$\begin{aligned}\sigma[P_{gg}(k_i,z_j)] &= \sqrt{F^{\rm dec\,-1}_{gg}(k_i,z_j)}\\ \sigma[P_{\Theta\Theta}(k_i,z_j)] &= \sqrt{F^{\rm dec\,-1}_{\Theta\Theta}(k_i,z_j)}\,. \quad (5)\end{aligned}$$

2.2 2D power spectra from mock map

We use the halo catalogue from the time-streaming mock map of the Horizon simulation (Teyssier et al. 2008), and cut 1 $(\mathrm{Gpc}/h)^3$ cubic box at the median redshift $\bar{z} = 0.83$, which contains 2.2 million halos. The fiducial cosmological parameters of the simulation are given by $(\Omega_m = 0.24, \Omega_k = 0, h = 0.72, \sigma_8 = 0.78, n_S = 0.96)$ and the initial transfer function is given by Eisenstein & Hu (1998).

The distribution of halos is modified according to their peculiar velocity to incorporate the redshift distortion effect. We adopt the distant observer approximation and measure the power spectrum in $(k_\perp, k_\parallel)$ space. The density fluctuation field is constructed by assigning the halos to 512^3 grids for the fast Fourier transformation (FFT) using the nearest grid point (NGP) method. Fig. 1 shows the resulting power spectrum. While linearly spaced bins in $(k_\perp, k_\parallel)$ are used in this plot for presentation purpose, we use bins in k and μ for the following analysis. k is divided in $\Delta k = 0.02\,h\,\mathrm{Mpc}^{-1}$ linearly equally spaced bins from $k = 0.02\,h\,\mathrm{Mpc}^{-1}$ to $0.2\,h\,\mathrm{Mpc}^{-1}$ and μ is in 5 linear-bins from 0 to 1 with equal spacing. The measured 2D power spectra in (k,μ) coordinate are shown in Fig. 2.

The Gaussian variance is used to derive errors for each bin shown as error bars in Fig. 2, $\sigma[\tilde{P}_{\rm ob}(k,\mu)] = \tilde{P}(k,\mu)\sqrt{2/N(k,\mu)}$ where $N(k,\mu)$ is number of modes in Fourier space. We test this using an alternative method, jack–knife errors (we do not attemp to generate more samples as we are interested in mocking real observables in a single patch). A total 64 jack–knife samples are prepared out of a single mock map by dividing each coordinate into 4 pieces.

$k(\,h\,\mathrm{Mpc}^{-1})$	0.03	0.05	0.07	0.09
$b(k)$	$1.65^{\pm 0.44}$	$1.70^{\pm 0.27}$	$1.60^{\pm 0.18}$	$1.69^{\pm 0.18}$

Table 1. Best fitting biases $b(k)$ at given scales k from $k = 0.03$ to $0.09\,h\,\mathrm{Mpc}^{-1}$.

Both errors agrees well, and different bins weakly correlate with each other.

Halo distribution is a biased tracer of the dark matter distribution. Theoretical $\tilde{P}_{\rm th}(k,\mu)$ from Kaiser effect only is given by,

$$\tilde{P}_{\rm th}(k,\mu) = b^2 P_{mm} + 2b\mu^2 r_{\rm h}\sqrt{P_{mm}P_{\Theta\Theta}} + \mu^4 P_{\Theta\Theta}\,, \quad (6)$$

where $P_{mm}(k)$ is the dark matter density–density spectra and $b = b(k)$ is the halo bias for each given scale. Spectra $P_{mm}(k)$ and $P_{\Theta\Theta}(k)$ are given from the cosmological parameters used for the simulation, and the halo cross–correlation parameter $r_{\rm h}$ is set to be unity. It has been tested that r for dark matter–Θ is perfectly correlated at linear scales $k < 0.1\,h\,\mathrm{Mpc}^{-1}$ from simulation. Unfortunately, the same sanity check is not applicable for halo maps due to the insufficient number of halo in each grid for direct velocity power spectra. Instead, the theoretical $\tilde{P}_{\rm th}(k,\mu)$ is derived based upon $r_{\rm h}(k) = 1$, and the possible departure from the unity is dectectable from measured $P_{\Theta\Theta}(k)$ at linear scales.

The tracer bias is assumed not to be determined by theoretical formalism or by other experiment. Instead of applying scale independent bias, $b(k)$ is varied independently for each k–bin. We fit $b(k)$ for each mode to get $\tilde{P}_{\rm th}(k,\mu)$ (solid curves in Fig. 2). In Table 1, the best fit $b(k)$ is given with 1–σ confidence level. Theoretical $\tilde{P}_{\rm th}(k,\mu)$ with fitted $b(k)$ is over–plotted with the measured $\tilde{P}_{\rm ob}(k,\mu)$ from the simulation in Fig. 2. We cut out scales $k < 0.03\,h\,\mathrm{Mpc}^{-1}$ due to our limited box size and $k > 0.1\,h\,\mathrm{Mpc}^{-1}$ due to non-linear effects.

Using $\tilde{P}_{\rm th}(k,\mu)$, theoretical errors are estimated from Fisher matrix analysis. Un-filled black contours in Fig. 3 represent the theoretical expectation around $b(k)^2 P_{mm}(k)$ and $P_{\Theta\Theta}(k)$. As it is prediced from halo bias model, measured bias is nearly scale independent.

2.3 Practical approach to extract peculiar velocity spectra

Spectra $P_{gg}(k_i)$ and $P_{\Theta\Theta}(k_i)$ are fitted simultaneously to $\tilde{P}_{\rm ob}(k_i,\mu_p)$ where i and p denote k and μ bins respectively. Bias is not parameterized to fit $\tilde{P}_{\rm ob}(k_i,\mu_p)$, instead, we use $P_{gg}(k_i)$. The fitting $\tilde{P}_{\rm fit}(k_i,\mu_p)$ is given by

$$\begin{aligned}\tilde{P}_{\rm fit}(k_i,\mu_p) &= \left[P_{gg}(k_i) + 2\mu_p^2\sqrt{P_{gg}P_{\Theta\Theta}} + \mu_p^4 P_{\Theta\Theta}(k_i)\right] \\ &\times\ G(k,\mu_j,\sigma_v)\,. \end{aligned} \quad (7)$$

We consider the velocity dispersion effect from one–dimensional velocity dispersion σ_v which is given by,

$$\left(\frac{\sigma_v}{aH}\right)^2 = \frac{1}{3\cdot 2\pi^2}\int P_{\Theta\Theta}(k,z)dk\,. \quad (8)$$

This formula needs $P_{\Theta\Theta}$ which is what we want to measure. We will discuss how we calculate this term in the next paragraph. Eq. 7 is expected to be invalidated beyond some threshold. The observed modes are cut out when it goes beyond given the threshold limit $\sigma_{\rm th}$ as $k_i\mu_{\rm cut}\sigma_v > \sigma_{\rm th}$. The fiducial value is $\sigma_{\rm th} = 0.24$ which represents confidence of theoretical prediction up to 6% drop of $G(k_i,\mu_{\rm cut},\sigma_v)$ from unity.

The most important factor in the integration Eq. 8 is the amplitude of $P_{\Theta\Theta}$, as scale–dependent factor of $P_{\Theta\Theta}$ is tightly constrained by CMB physics. The shape of the power spectra is determined before the epoch of matter–radiation equality. When the initial fluctuations reach the coherent evolution epoch after matter-radiation equality, they experience a scale-dependent shift from the moment they re-enter the horizon to the equality epoch. Gravitational instability is governed by the interplay between radiative pressure resistance and gravitational infall. The different duration of modes during this period results in a shape dependence on the power spectrum. This shape dependence is determined by the ratio between matter and radiation energy densities and sets the location of the matter-radiation equality in the time coordinate (Song et al. 2010).

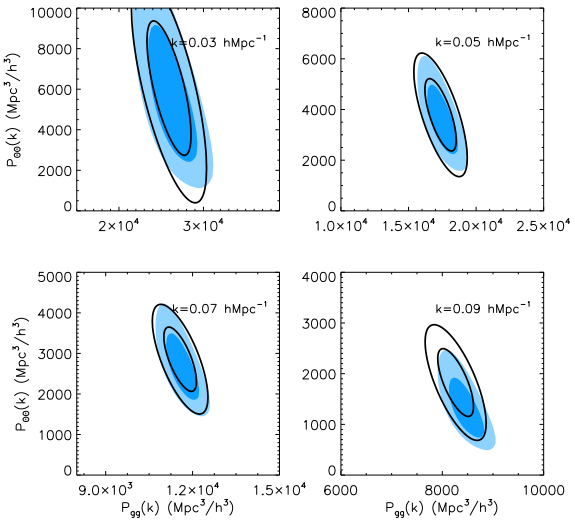

Figure 3. Contour plots are shown for decomposed $P_{gg}(k_i)$ and $P_{\Theta\Theta}(k_i)$ at $k = 0.03$, 0.05, 0.07 and $0.09\,h\,\mathrm{Mpc}^{-1}$. Unfilled black contours represent theoretical prediction from Fisher matrix analysis, and filled blue contours represent measured $P_{gg}(k_i)$ and $P_{\Theta\Theta}(k_i)$ from mock map in redshift space.

One way to estimate σ_v will be to use fitted $P_{\Theta\Theta}$ for each fitting step. Our measurement is, however, limited at scale of $k \lesssim 0.1\,h\,\mathrm{Mpc}^{-1}$ and the contribution to σ_v from $P_{\Theta\Theta}$ at $k \gtrsim 0.1\,h\,\mathrm{Mpc}^{-1}$ is small but not negligible ($\sim 10\%$). Therefore, we calculate σ_v using the linear shape of $P_{\Theta\Theta}$ with an amplitude which is estimated at each fitting step as follows.

For each $P_{\Theta\Theta}$ we want to test, we calculate the amplitude factor $g_\Theta(k_i,z)$ defined by

$$P_{\Theta\Theta}(k_i,z) = g_\Theta^2(k_i,z)P_{\Theta\Theta}(k_i,z_{\rm lss}), \quad (9)$$

and constrain the amplitude by calculating a weighted average of

$$\bar{g}_\Theta(z) = \frac{\sum_{i=i_{min}}^{i_{max}}\left(g_\Theta(k_i,z)/\sigma^2_{g_\Theta}(k_i,z)\right)}{\sum_{i=i_{min}}^{i_{max}} 1/\sigma^2_{g_\Theta}(k_i,z)}. \quad (10)$$

Here $\sigma_{g_\Theta}(k_i,z)$ is given by

$$\sigma_{g_\Theta}(k_i,z) = g_\Theta^{\rm fid}(k_i,z)\frac{\sigma[P^{\rm fid}_{\Theta\Theta}(k_i,z)]}{P^{\rm fid}_{\Theta\Theta}(k_i,z)}\,, \quad (11)$$

and $\sigma[P^{\rm fid}_{\Theta\Theta}(k_i,z_j)]$ is given by theoretical estimation in Eq. 5 and superscript 'fid' denotes the fiducial model for Fisher matrix analysis. We would not expect that fractional error of $P_{\Theta\Theta}(k_i,z)$ is much dependent on different fiducial models. The value of σ_v at the best fitted power spectra is $2.8\,h^{-1}$ Mpc (the linear theory prediction is $3.2\,h^{-1}$ Mpc).

$P_{gg}(k_i)$ determines the overall amplitude of $\tilde{P}_{\rm fit}(k_i,\mu_j)$, and $P_{\Theta\Theta}(k_i)$ determines the running of $\tilde{P}_{\rm fit}(k_i,\mu_j)$ in the μ direction. These distinct contribution allows us to separate information of $P_{gg}(k_i)$ and $P_{\Theta\Theta}(k_i)$ from 5 different μ bins at each k_i bin. We find these $P_{gg}(k_i)$ and $P_{\Theta\Theta}(k_i)$ by minimizing

$$\chi^2 = \sum_{i=i_{min}}^{i_{max}}\sum_{p=1}^{5}\sum_{q=1}^{5}[\tilde{P}_{\rm ob}(k_i,\mu_p)-\tilde{P}_{\rm fit}(k_i,\mu_p)] \times {\rm Cov}^{-1}_{pq}(k_i)[\tilde{P}_{\rm ob}(k_i,\mu_q)-\tilde{P}_{\rm fit}(k_i,\mu_q)]\,, \quad (12)$$

where $k_{i_{min}} = 0.03\,h\,{\rm Mpc}^{-1}$ and $k_{i_{max}} = 0.09\,h\,{\rm Mpc}^{-1}$. Off diagonal elements of the covariance matrix are nearly negligible and those diagonal elements are written as

$${\rm Cov}^{-1}_{pp}(k_i) = \frac{1}{\sigma[\tilde{P}_{\rm ob}(k_i,\mu_p)]^2}\,. \quad (13)$$

We present the difference between $\tilde{P}_{\rm th}(k_i,\mu_p)$ (Kaiser effect) and $\tilde{P}_{\rm fit}(k_i,\mu_p)$ (including dispersion effects) in Fig. 2. With the fiducial $\sigma_{\rm th} = 0.24$, only one bin of mode $k_i = 0.09\,h\,{\rm Mpc}^{-1}$ at $\mu_p = 0.9$ is removed from fitting. Altough this fitting procedure leads to correlations among different k bins through σ_v, those are minimally correlated and the results shown Fig. 3 are consistent with theoretical predictions.

3 RESULTS AND DISCUSSION

Velocity–velocity spectra are remarkably well extracted out of measured spectra in redshift space at scales $k = 0.03, 0.05$, and $0.07\,h\,{\rm Mpc}^{-1}$, and relatively well extracted at scale $k = 0.09\,h\,{\rm Mpc}^{-1}$ with more conservative confidence on the threshold limit. Filled blue contours in Fig. 3 represent fitted value of $P_{gg}(k_i)$ and $P_{\Theta\Theta}(k_i)$, and unfilled black contours represent estimation from theory with central values given by simulation. For scales from $k = 0.03$ to $0.07\,h\,{\rm Mpc}^{-1}$, the decomposed $P_{\Theta\Theta}(k_i)$ though our fitting strategy is trustable, which suggests that the few assumptions made in this paper are valid for those scales:

- The assumption of perfect correlation between halo distribution and velocity field is correct. The agreement of $P_{\Theta\Theta}(k_i)$ between fitted and true values supports our assumption of $r_h \sim 1$ indirectly.
- Dispersion effect is reasonably modelled at scales within our confidence limits, which enables us to extract $P_{\Theta\Theta}(k_i)$ in model independent way using estimated σ_v.

For $k = 0.09\,h\,{\rm Mpc}^{-1}$, more conservative threshold limits should be applied to remove non-linear supression. In Fig. 4, we present best fit $P_{\Theta\Theta}(k_i)$ with different threshold limits of $\sigma_{\rm th} = 0.24$ (left panel) and $\sigma_{\rm th} = 0.18$ (right panel). With $\sigma_{\rm th} = 0.24$, only one bin at $\mu_j = 0.9$ is removed. Shown in Fig. 2, extra suppression is also observed at $\mu_j = 0.7$ bin at $k = 0.09\,h\,{\rm Mpc}^{-1}$ which can be removed by more conservative bound $\sigma_{\rm th} = 0.18$. Shown in the right panel of Fig. 4, true $P_{\Theta\Theta}(k_i)$ is restored at the cost of weakened constraint.

Theoretical estimation from Fisher matrix analysis is an optimistic bound on errors. It is noticeable that measured varinaces (filled blue contours in Fig. 3) are consistent with estimated variances (unfillled black contours in Fig. 3), which assures us that our method is optimized extraction of $P_{\Theta\Theta}(k_i)$ for the given simulation specification.

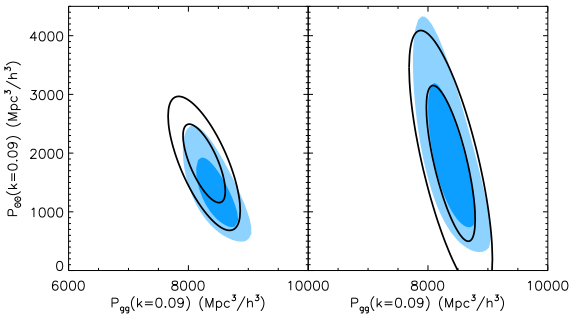

Figure 4. Contour plots are shown for decomposed $P_{gg}(k_i)$ and $P_{\Theta\Theta}(k_i)$ at $k = 0.09\,h\,{\rm Mpc}^{-1}$ with $\sigma_{\rm th} = 0.24$ (left panel) and 0.18 (right panel). Unfilled black and filled blue contours represent the same in Fig. 3.

4 CONCLUSION

We propose a statistical tool to decompose $P_{gg}(k)$ and $P_{\Theta\Theta}(k)$ practically out of redshift distortion maps, with a few assumptions: 1) perfect correlation between density and velocity fluctuations, 2) confidence on theoretical prediction of velocity dispersion effect within threshold limit. The results show that the true value of velocity–velocity spectra up to $k = 0.07\,h\,{\rm Mpc}^{-1}$ are successfully recovered using theoretical dispersion effect. The detectability is extendable up to $k \sim 0.1\,h\,{\rm Mpc}^{-1}$ with more conservative threshold limit at the cost of weakened constraint. We find that the theoretical dispersion effect can be estimated from $P_{\Theta\Theta}(k)$ parameters using weighted average at $k < 0.1\,h\,{\rm Mpc}^{-1}$. In linear regime, $P_{\Theta\Theta}(k)$ is well–measured with this estimated σ_v as much as with the true fixed σ_v of the simulation.

We find that the biased measurement of $P_{\Theta\Theta}(k)$ is mainly caused by the unpredictable non–linear supression effect at $k > 0.1\,h\,{\rm Mpc}^{-1}$. The detectability limit in scale can be extended by parameterizing this effect (Tang et al. 2010), but we scope our range of interest in linear regime in this paper.

ACKNOWLEDGMENTS

We would like to thank Romain Teyssier for offering simulation map of Horizon (*http://www.projet-horizon.fr*), and to thank Prina Patel for comment on the manuscript. Y-S.S. is supported by STFC and I.K. acknowledges support by JSPS Research Fellowship and WPI Initiative, MEXT, Japan.

REFERENCES

Bean R., Tangmatitham M., 2010
Colless M. e., 2003, ArXiv Astrophysics e-prints
Davis M., Peebles P. J. E., 1982, Astrophys. J., 267, 465
Eisenstein D. J., Hu W., 1998, ApJ, 496, 605
Fisher K. B., 1995, ApJ, 448, 494
Fisher K. B., Scharf C. A., Lahav O., 1994, MNRAS, 266, 219
Garilli B. e., 2008, A&A, 486, 683
Gaztanaga E., Cabre A., 2008, ArXiv e-prints
Guzik J., Jain B., Takada M., 2010, Phys. Rev., D81, 023503
Guzzo L., et al., 2008, Nature, 451, 541
Hamilton A. J. S., 1992, ApJL, 385, L5
Hawkins E. e., 2003, MNRAS, 346, 78

Kaiser N., 1987, MNRAS, 227, 1
Lahav O., Lilje P. B., Primack J. R., Rees M. J., 1991, MNRAS, 251, 128
Le Fèvre O. e., 2005, A&A, 439, 877
Lilje P. B., Efstathiou G., 1989, MNRAS, 236, 851
Linder E. V., 2008, Astropart. Phys., 29, 336
McDonald P., Seljak U., 2009, JCAP, 0910, 007
McGill C., 1990, MNRAS, 242, 428
Okumura T. e., 2008, ApJ, 676, 889
Peacock J. A. e., 2001, Nature, 410, 169
Percival W. J., White M., 2008
Percival W. J. e., 2004, MNRAS, 353, 1201
Pueblas S., Scoccimarro R., 2009, Phys. Rev. D, 80, 043504
Scoccimarro R., 2004, Phys. Rev. D, 70, 083007
Simpson F., Peacock J. A., 2009
Song Y.-S., Percival W. J., 2009, JCAP, 0910, 004
Song Y.-S., Sabiu C. G., Nichol R. C., Miller C. J., 2010, JCAP, 1001, 025
Stril A., Cahn R. N., Linder E. V., 2009
Tang J., Kayo I., Takada M., 2010, *Prepared*
Taruya A., Nishimichi T., Saito S., Hiramatsu T., 2009, Phys. Rev. D, 80, 123503
Tegmark M. e., 2006, Phys. Rev. D, 74, 123507
Teyssier R., et al., 2008
Wang Y., 2008, JCAP, 0805, 021
White M., Song Y.-S., Percival W. J., 2009, MNRAS, 397, 1348
York D. G. e., 2000, AJ, 120, 1579
Zehavi I. e., 2005, ApJ, 630, 1